Final technical report

COLLABORATIVE RESEARCH ON ECOPHYSIOLOGICAL CONTROLS ON AMAZONIAN PRECIPITATION SEASONALITY AND VARIABILITY

Award number: DE-SC0011113

The goal of the Carnegie Institution's part of this work was to investigate the potential for using solar induced fluorescence (SIF) measurements to inform on vegetation phenology and physiological stress associated with the wet season and dry seasons in Amazonia. Dr. Ari Kornfeld working in Joe Berry's lab has focused on developing the instrumentation to measure chlorophyll fluorescence from flux towers in the Amazon.

Interest in measuring solar induced chlorophyll fluorescence (SIF) has been growing over the past several years, following reports that satellite-based SIF retrievals can be used as a proxy for global primary productivity (GPP), (Joiner et. al., 2011; Frankenberg et al., 2011). Chlorophyll fluorescence is the reemission, at a longer wavelength, of photons absorbed by chlorophyll pigments. At the membrane level 1-5% of absorbed light is reemitted as fluorescence. Much of this is reabsorbed before exiting the top of the canopy. Upwelling SIF is measured by comparing a downwelling solar spectrum to the light upwelling from the canopy. The reflected light preserves the fine spectral structure of the solar spectrum, whereas the fluorescence spectrum is spectrally smooth (Figure 1). Current satellite retrievals use solar Fraunhofer lines in a band adjacent to the O_2A band (745 – 759 nm; Figure 1). We have chosen to use the solar lines in our design to maintain continuity with the satellite measurements. Most ground-based SIF measurements are made in the O_2A band (Meroni et. al., 2009) which is a much deeper absorption feature, but it is subject to interference by anything that changes the light's path length through Earth's atmosphere, requiring near simultaneous measurement of upwelling and downwelling spectra. Further, O2 in the atmosphere between the sensor and the canopy can attenuate the fluorescence signal (Liu et al., 2017). The weaker Fraunhofer features are more robust, but require a combination of higher spectral resolution and higher signal/noise ratio (SNR), therefore, we have given a lot of attention to the design of our light collection system.

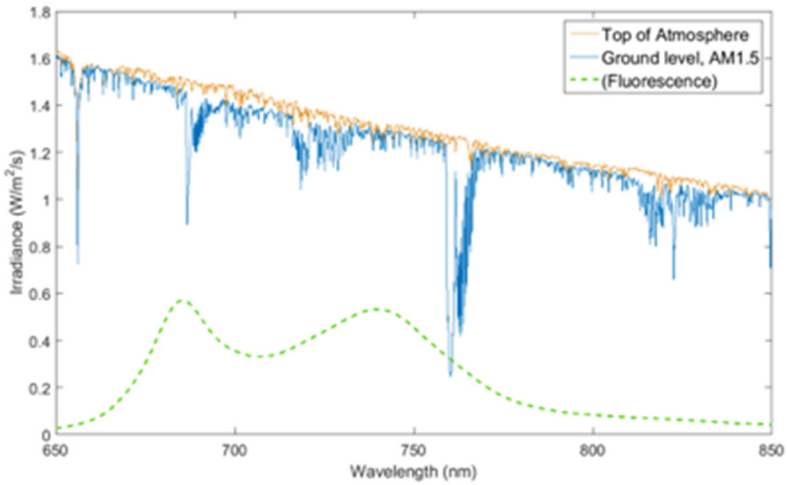

Figure 1. The chlorophyll fluorescence spectrum (dashed-green) is smooth relative to the solar radiation spectrum (gold: top of atmosphere, blue: ground-level). The amplitude of the fluorescence spectrum is greatly exaggerated, for comparison purposes.

Several tower-based systems have recently been described for measuring SIF (Frankenberg et al., 2018; Yang et al., 2018). Here we describe a novel tower-based SIF instrument designed to have a robust optical path while allowing the instrument to operate unattended over long intervals in weather characteristic of Amazonia. The key piece of our design is a foreoptic we have named "rotoprism".

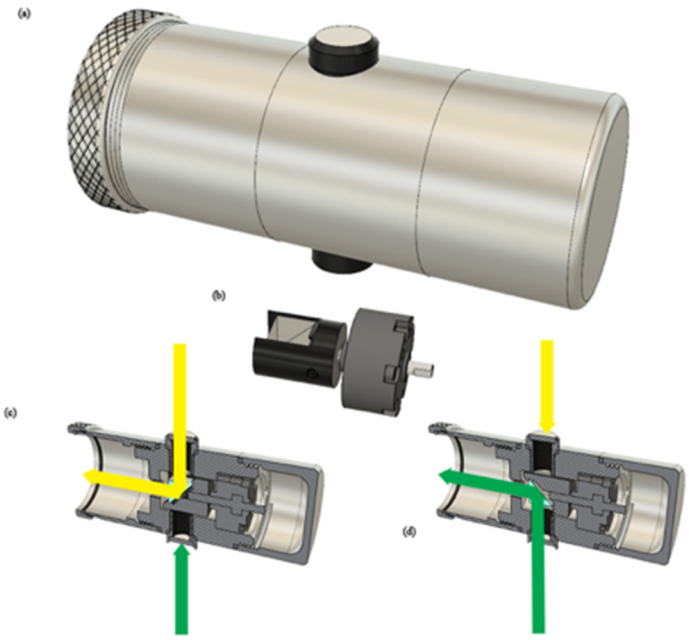

Figure 2. Diagram of rotaprism. (a) fully assembled: the device is 15 cm long by 5 cm in diameter. (b) rotor and actuator. (c, d) cut-away view, showing the rotating prism selecting between downwelling (c) and upwelling (d) light. The horizontal beam is directed to an optical fiber by a collimating lens in the exit gap (c and d), not shown.

This device is connected to a spectrometer via a fiber optic (Figure 3). A prism selects whether the fiber is collecting light that is downwelling from the sun or reflected upward from the canopy. This is accomplished by an actuator that rotates an internal prism through 180 degrees to select between upward- and downward-looking windows (Figure 2b). The prism reflects the light from the selected diffuser into a collimating lens attached to a horizontally-facing optical fiber. The directional sensitivity of the rotoprism with diffusing windows made of opal glass follows the cosine law. Therefore, the fiber samples the net upwelling or downwelling light at the top of canopy. These optical components are contained in a three-part aluminum body consisting of a pipe-adapter, the main body with axial optical windows, and a cap (Figure 2). A threaded hole in the base of the main body accepts a collimating lens for attaching the fiber (not visible in Figure 3). The threads on this

adapter are compatible with the standard SMA convention used in the fiberoptics market. We use collimating lenses from spectrometer manufacturers such as Ocean Optics (Largo, Florida) or Avantes (Apeldoorn, The Netherlands). The distal-end of the main body supports the actuator with the rotating prism assembly, and is sealed with an aluminum cap (right end of Figure 3a). The pipe adapter (left end of Figure 3a), which can be customized to fit any diameter support pipe; the design shown here fits over an ASTM 1 ¼" pipe. A threaded aluminum collar with an internal O-ring screws onto the end of the pipe adapter to provide a friction-seal to affix the entire assembly to a horizontal support pipe (far-left end of Figure 3a). Optical and pneumatic tubes run through the pipe; two axial holes along the sides of the main body provide an internal path for the pneumatic tubes to reach the actuator, thus providing end-to-end protection for all lines running from the spectrometer to the foreoptic. Radial optical-window holders ("inserts") and the prism holder are machined from PPO/Noryl plastic. An optical disk – diffuser or a lens – is glued into the seat of the optical-window holders to form a water-tight seal. The inserts are threaded to allow windows or lenses to be easily swapped without affecting optical alignment. Flat rubber gaskets between insert and body ensure water tightness. The prism holder (Figure 3b) holds the hypotenuse of the prism at a 45 degree angle; an axial bore fits onto the shaft of the pneumatic rotary actuator (SMC Pneumatics, part NCRB1BW10-180SE), which is inserted into the central aluminum body from its distal end (Figure 3c, d). The CNC code for all of the machined parts plus a complete list of components is available on request. The entire assembly is water-tight as tested by immersion into water overnight. In the field the rotoprism is mounted on the end of an aluminum pipe supported from the tower approximately 20 m above the top of the forest canopy. The spectrometer is located in an airconditioned shed at the bottom of the tower.

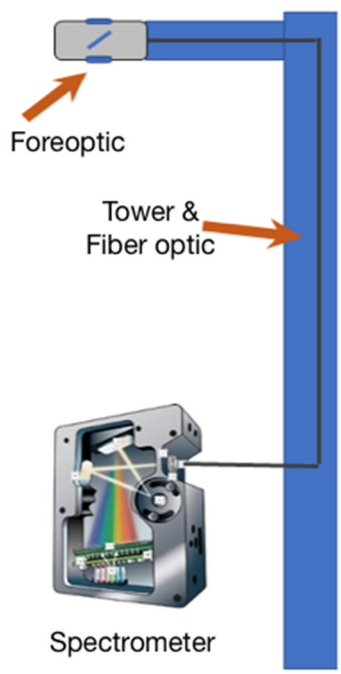

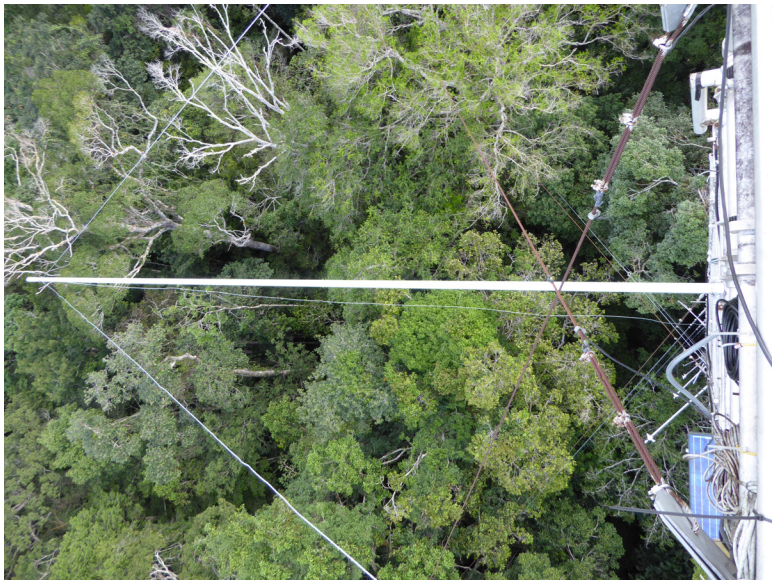

Figure 3. The light collection system as deployed at the K34 tower showing the rotoprism at the end of the mounting pipe (top left); a schematic of the setup (top right), and a view of the deployed rotoprism from the top of the tower.

Fibers and Spectrometer subsystems. An 80 meter, SMA-terminated optical fiber bundle (Fiberoptic Systems, USA) connects the rotaprism's optical output to the spectrometer. The fiber can direct light to any number of spectrometers. In our standard configuration the bundle contains two fibers: a 600 μ, low-OH fused-silica fiber connected to a high-resolution, thermo-electrically cooled grating spectrometer (QE Pro, Ocean Optics) used for the SIF retrievals, and a 200 μ, low-OH fiber connected to a lower spectral resolution broadband spectrometer (Flame, Ocean Optics), used for determining vegetation indexes and PAR estimates. Attenuation of the optical signal in the fiberoptic is trivial (~10%/100 m). Both spectrometers are maintained at a constant temperature to +/- 0.5 C, in a custom-built thermo-electrically cooled enclosure. The QE Pro used for the experiments described here provides spectral resolution of 0.15 nm FWHM from 730 – 785 nm (0.05 nm dispersion). The Flame spectral resolution is 1.1 nm FWHM for 350 – 1000 nm (0.33 nm dispersion). Two 1/8" OD urethane pneumatic tubes (Clippard, USA) connect the rotary actuator to pneumatic solenoid valves. The solenoid valves are controlled via software, using the spectrometer's digital output ports connected to solid state relays to turn them on and off. These components are controlled by a laptop computer

with software described below.

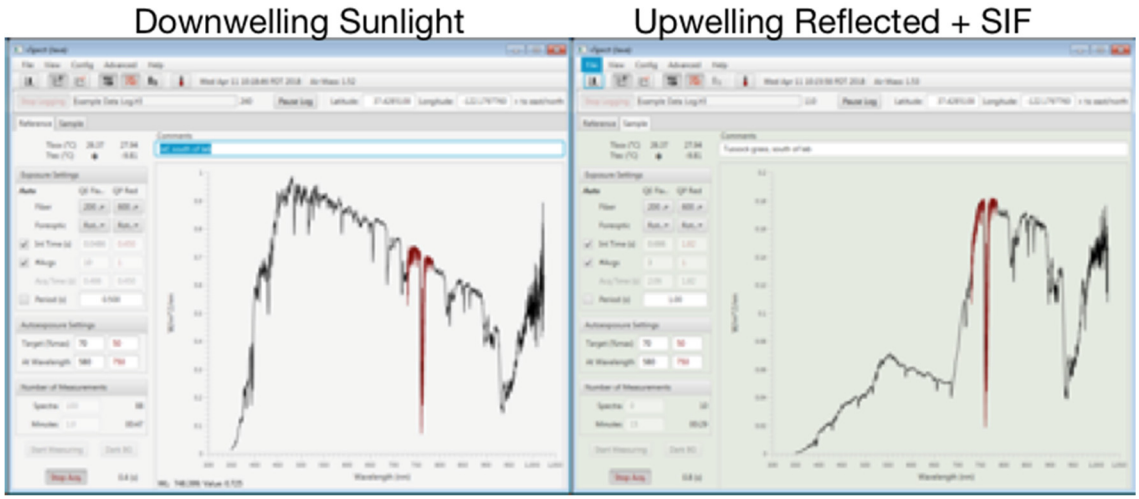

Figure 4. Typical spectra collected by the Flame (black) and QE Pro (red) spectrometers. The Flame spectrometer covers the range from 350 to 1000 nm at 1.1 nm FWHM and the QE Pro from 730-780 nm with 0.15 nm FWHM. The cross calibration of the two spectrometers is such that their output is identical in the region of overlap.

Retrieval. SIF can be retrieved from upwelling light because the shape of the chlorophyll fluorescence spectrum is markedly different than the upwelling reflected light. The reflected light preserves the fine spectral structure of the solar spectrum, whereas the fluorescence spectrum is spectrally smooth (Figure 1). The contrast between these two spectral components is what allows a regression model to separate the two sources.

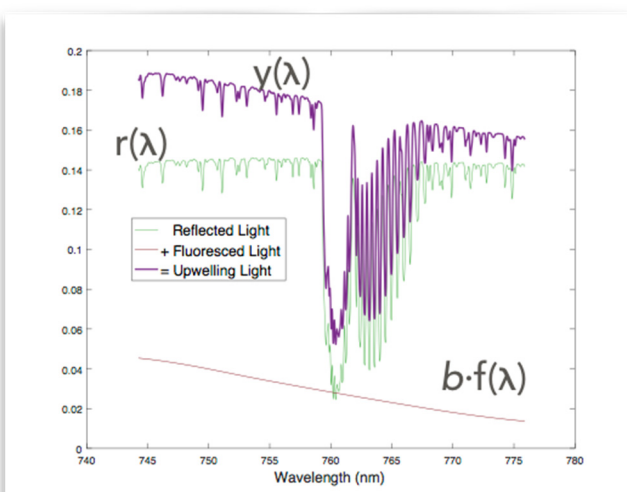

Figure 5. High resolution spectra in the waveband used for SIF retrieval (re-drawn with an exaggerated fluorescence contribution, $f(\lambda)$. The observed spectrum, $y(\lambda)$ is the sum of $f(\lambda)$ and the reflected light, $r(\lambda)$ which is the product of the canopy reflectance $r(\lambda)$ and the

downwelling solar. $s(\lambda)$. A regression is used to invert an observed spectrum, knowing $r(\lambda)$, $s(\lambda)$ and $f(\lambda)$ for the terms a and b that indicate the fraction of reflected and fluorescence light, respectively.

Mathematically, the intensity of the upwelling light at wavelength λ, y(λ) (assuming no atmospheric absorption between the canopy and the detector), is:

$$y(\lambda) = a\, r(\lambda)\, s(\lambda) + b\, f(\lambda), \quad \text{Eqn. 1}$$

where $y(\lambda)$ is the scaled sum of two spectral shapes: (1) the upwelling reflected light, computed as the product of downwelling radiation at the top of canopy, $s(\lambda)$ and the canopy reflectance, $r(\lambda)$ and (2) the fluorescence emissions, $f(\lambda)$. If the three spectral shape functions $r(\lambda)$, $s(\lambda)$, and $f(\lambda)$ are standardized to equal one at a specified wavelength, then the coefficients a, and b, represent the absolute intensity of reflected and fluoresced light at that wavelength. For the purposes of retrieval (the inverse model), the shapes of $r(\lambda)$, $s(\lambda)$, and $f(\lambda)$ are considered to be "known" values because they are either measured, modeled or prescribed. $r(\lambda)$ can also be prescribed or it can be approximated as a polynomial or other function of λ, with coefficients to be determined simultaneously with a and b, in the statistical regression. A variety of retrieval methods have been proposed (Meroni et al., 2009). Here we use a method described by Guanter et al. (2013), sometimes referred to as the "SVD" method where $s(\lambda)$ is reconstructed from the scaled sum of singular vectors produced from the singular value decomposition (SVD) of many samples of downwelling measurements recorded over the course of a day. The function produces a statistically validated representation of the downwelling spectrum at any time during the day of sampling. This approach minimizes noise in the reference spectrum and eliminates the need to have simultaneous upwelling and downwelling spectra (Gao et. al., 2019). Samples of the downwelling light are routinely analyzed for the apparent level of SIF (SIF should be zero) as a control on the accuracy of the analysis.

Software. We designed a software suite with independent programs for data acquisition and data analysis. The data acquisition program, written in Java, is named xSpect. It provides fault-tolerant control of the data acquisition, computes ideal exposure times, coordinates the spectrometers and the foreoptic, and records data for subsequent analysis. xSpect includes a graphical user interface (GUI) offering a variety of options for automated or manual data acquisition, for viewing and diagnosing spectral output, and for storing the data and metadata in HDF5 files.

During data acquisition raw DN (digital numbers) are corrected for pixel-independent detector nonlinearity using a polynomial function supplied by the factory or user-supplied. However, to further minimize nonlinearity effects, acquisition times are adjusted ("auto-exposure") so that the DN remain within a user-determined range corresponding to the "flattest" part of the linearity curve (50% of max DN for the QE Pro; 70% of max DN for the Flame, user adjustable). The default spectral window for auto-exposure is centered on 750 nm for the SIF spectrometer, and 580 nm for the broadband spectrometer.

In addition to performing the nonlinearity correction, dark current is subtracted from each acquired spectrum before recording. To facilitate the auto-exposure function, dark current is computed in a two-step process: first, all spectra are corrected by subtracting the mean DN of opaque pixels built into the detector. This correction minimizes effects of temperature and integration time but cannot account for pixel-to-pixel variation. The second correction is based on per-pixel calibration factors derived in advance by capping the spectrometer and recording DN reported for each pixel at various integration times, at acquisition temperature. A polynomial function of dark DN as a function of integration time is computed for each pixel. For the Ocean Optics spectrometers mentioned here, a linear function suffices. Once saved, the dark correction factors are automatically associated with each spectrometer. When using the software interactively, one can also record dark spectra immediately before conduction measurement rather than using the computed dark spectra. In this case, the recorded dark spectrum is considered valid until the integration time changes.
To provide relatively uniform capture intervals, as well as to account for integration-time differences across spectrometers, the software may average several spectra before recording to the data file. In addition to integration time, software provides options specifying whether and for how long the it should direct the foreoptic to measure upwelling and downwelling light.

Newly acquired data are checked to ensure that the actuator was correctly positioned, and a warning is flagged if the test fails. Recording is automatically paused according to a variety of criteria including solar angle, light level and/or time of day. Metadata recorded with each spectrum includes acquisition time, acquisition parameters, internal temperatures reported by the spectrometers, upwelling/downwelling classification, associated calibration factors, dark factors. A user comment may also be associated with each spectrum. Additional data includes location and spectrometer type and configuration. The data are stored in an HDF5 file, in a format optimized to reduce size without sacrificing data quality.

The data analysis program, called SIFviewer, provides a visual interface for retrieving SIF, diagnosing data quality and computing spectrometer calibration factors. The software is written in MATLAB but does not require knowledge of MATLAB, nor a MATLAB license, to run in pre-compiled mode. SIF is computed using the "SVD" method (Guanter, L. et al., 2013). The function is very similar to the curve used in the SCOPE model (van der Tol et al., 2009) and reported in a previous study (Magney et al., 2017). In order to reduce or avoid heteroschedasticity, the regression is performed on DN/s data rather than irradiance, which multiplies both signal and noise by pixel-specific coefficients. The fluorescence function, $f(\lambda)$, is therefore converted to DN/s by dividing $f(\lambda)$ by the calibration coefficients associated with each recorded spectrum.

The SIFviewer GUI allows one to set retrieval parameters including retrieval band, the polynomial degrees, the number of singular values to use, and the type of regression: linearized or nonlinear. The user can then visually inspect the spectra, the singular vectors, the computed SIF, the components of

the regression, the residuals, additional reflectance indices (if broadband data are available), and various diagnostic graphs. The program also generates intensity- and dark-current- calibration factors from recorded data. Spectrometers/fiber pairs are calibrated for irradiance using an Avantes HAL-CAL-SMA NIST-traceable calibrated light source. Foreoptics are calibrated independently of the spectrometer by computing spectral transmission using an integrating sphere. Spectrometer and foreoptic calibrations are user-selectable through the GUI or in a configuration file. During data acquisition, calibration factors are computed as the product of spectrometer and foreoptic coefficients. The intensity calibration vector is stored in data-acquisition metadata and associated with each corresponding spectrum. The software developed for this project can be made available on request.

Results. A plot of measurements over a typical day (Figure 6) shows the very strong correlation of SIF (filled circles) with downwelling solar radiance.

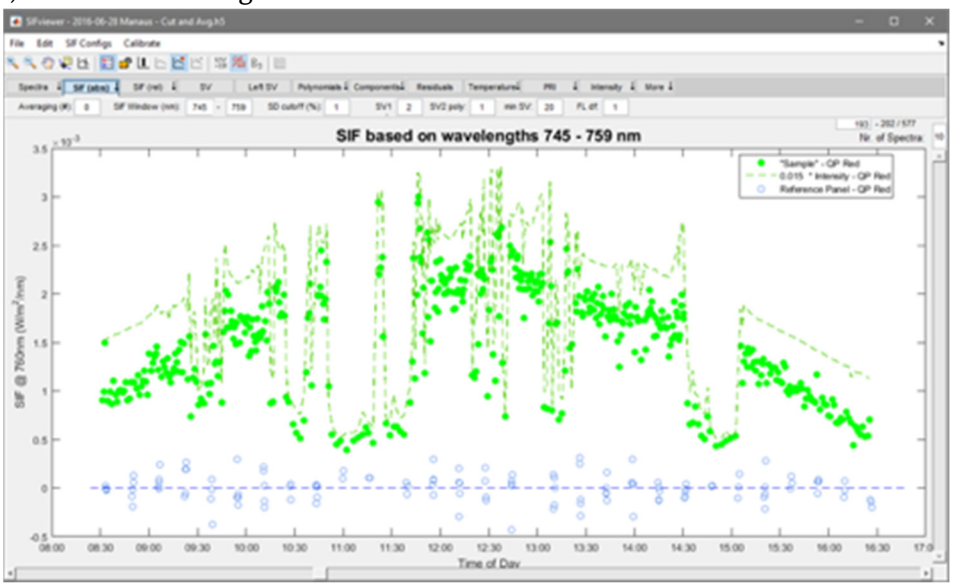

Figure 6. Measurements (averaged to 5 min) over a typical day at the K34 tower near Manaus Brazil. The dashed line shows the course of downwelling solar (scaled for comparison) , SIF is the filled, green points, and the reference calculation are the reference points.

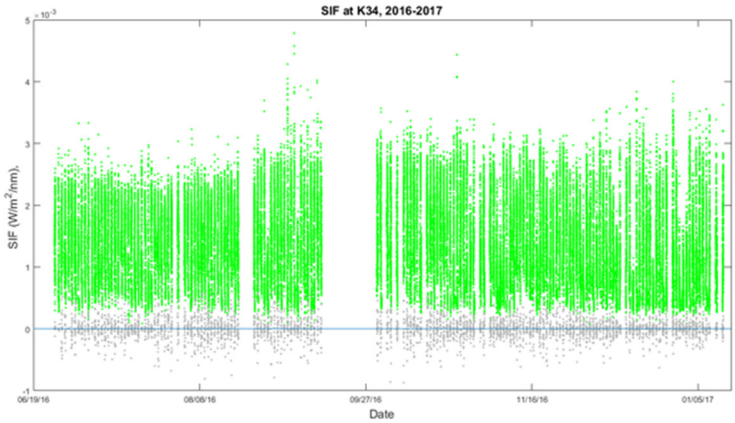

Figure 7. SIF data collected on 170 days over the period June 19, 2016 to Jan 15, 2019. Gaps in the data stream were primarily due to power outages.

The rotoprism installation was robust and remained fully functional throughout the deployment. Gas for the actuator was supplied by a tank of compressed N_2. We estimate that the system can run for a year on a single K size tank of commercial N_2. The monitoring was terminated when the air conditioning of the instrument shack failed. This led to overloading of the thermoelectric temperature control system and damage to the electronics. We were not able to repair the temperature regulation system and without a reliable air conditioning system we abandoned the site. The data stream spanned nearly a complete dry season (Fig 7.).

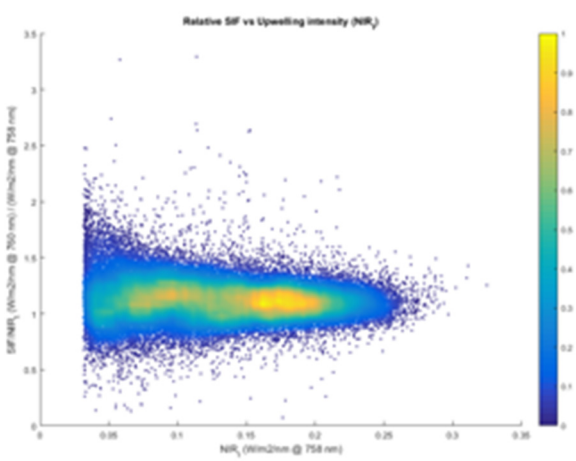

Figure 8. The SIF radiance was highly correlated with the downwelling solar radiance at 758 nm. This plot shows the ratio SIF/downwelling solar at 758 nm.

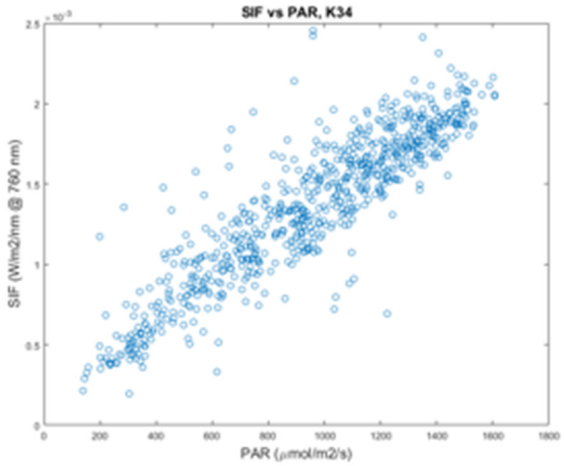

Figure 9. SIF was strongly correlated with measured photosynthetically active radiation (PAR) from a LiCor quantum probe (both integrated to half hourly intervals), R2= 0.81.

SIF is the re-emission of absorbed PAR. Scatter is likely due to differential responses fluorescence yield and canopy radiation transport to diffuse and direct solar radiation.

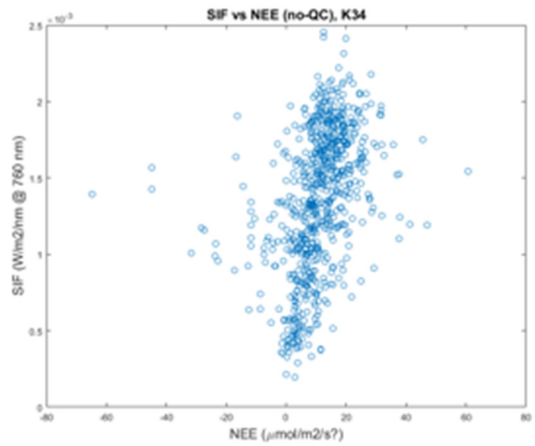

Figure 10. SIF plotted vs. net ecosystem exchange (half hourly) measured by eddy covariance at the K34 tower (courtesy A.) Note that the NEE data does not extend for the full time span of the SIF measurements.

SIF is often proposed as a proxy for photosynthesis. Here we show that there is an adequate correlation that is similar in this case to the independent correlation of NEE with incident PAR. This dense canopy did not show any detectable change in fluorescence properties that might be attributed to water stress over the course of the dry season. There has been considerable interest in the possibility first suggested by Saleska et al. (2012) that the Amazon forest greens up during the dry season. This has largely been based on measurements of various vegetation indices that use reflected light. These can be sensitive to contamination by light reflected from other objects unrelated to leaves (soil, tree bolls, clouds, atmospheric aerosols, etc.). SIF is absolutely specific to green leaves.

Therefore, we examined our SIF data to see if there is evidence of canopy greening during the dry season. Our analysis (Figure 11) shows considerable scatter but a significant trend of 3.4% (p=0.0024) in the ratio of emitted SIF to upwelling NIR radiance. We interpret this as a change either in the number of leaves displayed by the canopy or in the leaf angle distribution.

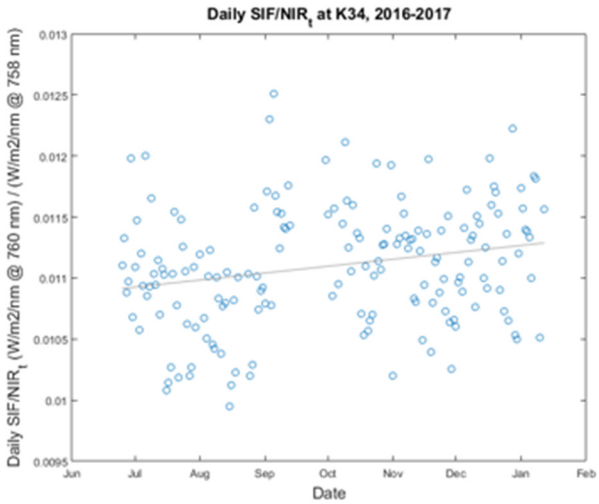

Figure 11. Change in the daily means of relative SIF over the dry season at K34. Note that the expanded vertical axis. The trend line is significant and represents an increase of 3.4% over the course of 16-17 dry season.

Conclusions.

We developed a robust and accurate system for measurement of SIF.

This system was successfully deployed at the K34 tower near Manaus.

We conducted measurement over 190 days.

The SIF emission normalized to the downwelling radiance was stable over this time, showing no effect of water stress. There was a small (3.4%) increase in SIF over the dry season presumably related to growth of new leaves at the top of the canopy. The area probed by the sensor may not have been representative of the overall canopy.

References

Atherton J, Nichol CJ, Porcar-Castell A. 2016. Using spectral chlorophyll fluorescence and the photochemical reflectance index to predict physiological dynamics. *Remote Sensing of Environment* **176**: 17-30.

Daumard F, Champagne S, Fournier A, Goulas Y, Ounis A, Hanocq JF, Moya I. 2010. A Field Platform for Continuous Measurement of Canopy Fluorescence. *Ieee Transactions on Geoscience and Remote Sensing* **48**(9): 3358-3368.

Frankenberg C, Kohler P, Magney TS, Geier S, Lawson P, Schwochert M, McDuffie J, Drewry DT, Pavlick R, Kuhnert A. 2018. The Chlorophyll Fluorescence Imaging Spectrometer (CFIS), mapping far red fluorescence from aircraft. *Remote Sensing of Environment* **217**: 523-536.

Grossmann K, Frankenberg C, Magney TS, Hurlock SC, Seibt U, Stutz J. 2018. PhotoSpec: A new instrument to measure spatially distributed red and far-red Solar-Induced Chlorophyll Fluorescence. *Remote Sensing of Environment* **216**: 311-327.

GU, L., Han, J., Wood, J. D., Chang, C. Y. Y., & Sun, Y. (2019). Sun-induced chlorophyll fluorescence and its importance for modeling photosynthesis from the side of light reactions. New Phytologist, nph.15796–43. http://doi.org/10.1111/nph.15796

Guanter L, Frankenberg C, Dudhia A, Lewis PE, Gomez-Dans J, Kuze A, Suto H, Grainger RG. 2012. Retrieval and global assessment of terrestrial chlorophyll fluorescence from GOSAT space measurements. *Remote Sensing of Environment* **121**: 236-251.

Guanter L, Rossini M, Colombo R, Meroni M, Frankenberg C, Lee J-E, Joiner J. 2013. Using field spectroscopy to assess the potential of statistical approaches for the retrieval of sun-induced chlorophyll fluorescence from ground and space. *Remote Sensing of Environment* **133**: 52-61.

Guanter L, Rossini M, Colombo R, Meroni M, Frankenberg C, Lee JE, Joiner J. 2013. Using field spectroscopy to assess the potential of statistical approaches for the retrieval of sun-induced chlorophyll fluorescence from ground and space. *Remote Sensing of Environment* **133**: 52-61.

Joiner J, Guanter L, Lindstrot R, Voigt M, Vasilkov AP, Middleton EM, Huemmrich KF, Yoshida Y, Frankenberg C. 2013. Global monitoring of terrestrial chlorophyll fluorescence from moderate-spectral-resolution near-infrared satellite measurements: methodology, simulations, and application to GOME-2. *Atmospheric Measurement Techniques* **6**(10): 2803-2823.

Kautsky H, Hirsch A. 1934. Chlorophyll-fluorescence and carboxylic acid assimilation. I. Announcement: The fluorescence performance of green plants. *Biochemische Zeitschrift* **274**: 423-434.

Li X, Xiao JF, He BB, Arain MA, Beringer J, Desai AR, Emmel C, Hollinger DY, Krasnova A, Mammarella I, et al. 2018. Solar-induced chlorophyll fluorescence is strongly correlated with terrestrial photosynthesis for a wide variety of biomes: First global analysis based on OCO-2 and flux tower observations. *Global Change Biology* **24**(9): 3990-4008.

Liu XJ, Liu LY, Hu JC, Du SS. 2017. Modeling the Footprint and Equivalent Radiance Transfer Path Length for Tower-Based Hemispherical Observations of Chlorophyll Fluorescence. *Sensors* **17**(5): 15.

Magney TS, Frankenberg C, Fisher JB, Sun Y, North GB, Davis TS, Kornfeld A, Siebke K. 2017. Connecting active to passive fluorescence with photosynthesis: a method for evaluating remote sensing measurements of Chl fluorescence. *New Phytologist* **215**(4): 1594-1608.

Meroni M, Rossini M, Guanter L, Alonso L, Rascher U, Colombo R, Moreno J. 2009. Remote sensing of solar-induced chlorophyll fluorescence: Review of methods and applications. *Remote Sensing of Environment* **113**(10): 2037-2051.

Porcar-Castell A. 2011. A high-resolution portrait of the annual dynamics of photochemical and non-photochemical quenching in needles of Pinus sylvestris. *Physiologia Plantarum* **143**(2): 139-153.

Schreiber U. 1983. Chlorophyll fluorescence yield changes as a tool in plant physiology .1. the measuring system. *Photosynthesis Research* **4**(4): 361-373.

Schreiber U, Schliwa U, Bilger W. 1986. Continuous recording of photochemical and nonphotochemical chlorophyll fluorescence quenching with a new type of modulation fluorometer. *Photosynthesis Research* **10**(1-2): 51-62.

van der Tol C, Verhoef W, Timmermans J, Verhoef A, Su Z. 2009. An integrated model of soil-canopy spectral radiances, photosynthesis, fluorescence, temperature and energy balance. *Biogeosciences* **6**(12): 3109-3129.

Yang X, Shi HY, Stovall A, Guan KY, Miao GF, Zhang YG, Zhang Y, Xiao XM, Ryu Y, Lee JE. 2018. FluoSpec 2-An Automated Field Spectroscopy System to Monitor Canopy Solar-Induced Fluorescence. *Sensors* **18**(7): 18.

Zhou XJ, Liu ZG, Xu S, Zhang WW, Wu J. 2016. An Automated Comparative Observation System for Sun-Induced Chlorophyll Fluorescence of Vegetation Canopies. *Sensors* **16**(6): 15.